Abstract: Comprehensive studies for a periodic array of gold nanorod pairs demonstrate its unique optical properties, including a negative refractive index in the optical range.

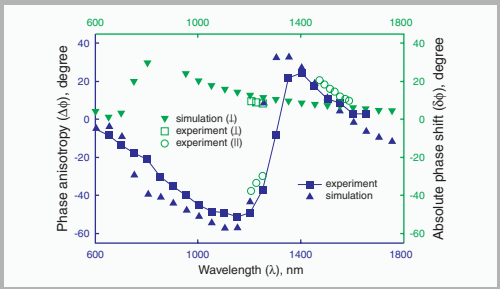

Phase difference in transmission through the layer of pairs of gold rods of Sample A, for light polarized parallel and perpendicular to the rods

Experimental verification of an optical negative-index material

V.P. Drachev, [1] *W. Cai,* [1] *U. Chettiar,* [1] *H.-K. Yuan,* [1] *A.K. Sarychev,* [2] *A.V. Kildishev,* [1] *G. Klimeck,* [3] *and V.M. Shalaev* [1,*]

[1] School of Electrical & Computer Engineering, Purdue University, West Lafayette, IN 47907, USA
[2] Ethertronics Inc., 9605 Scranton Road, San Diego, CA 92121, USA
[3] Network for Computational Nanotechnology, Discovery Park, Purdue University, IN 47907, USA

Received: 24 September 2005, Accepted: 28 September 2005
Published online: 13 October 2005

Key words: negative index material; negative refraction; interferometry

PACS: 78.20.-e, 78.20.Bh

1. Introduction

Artificially designed materials (metamaterials) with a negative refractive index allow the achievement of new functionality unattainable with naturally-existing media [1], including the feasibility of imaging with subwavelength resolution limited by only the material quality [2]. In these negative-index materials (NIMs) the phase velocity is antiparallel to the energy flow leading to the unusual effect of negative refraction at the interface with a conventional, positive refractive index medium. The seminal paper defining a method toward a negative refractive index was published in the 1960s [3]. In media characterized by dielectric permittivity $\varepsilon = \varepsilon' + i\varepsilon''$ and magnetic permeability $\mu = \mu' + i\mu''$ the condition $\varepsilon' < 0$ and $\mu' < 0$ is sufficient for negative refraction [3]. Under the necessary condition $\varepsilon''\mu' + \mu''\varepsilon' < 0$ [4], the real part (n') of the complex refractive index ($n = n' + in'' = \sqrt{\varepsilon\mu}$) becomes negative

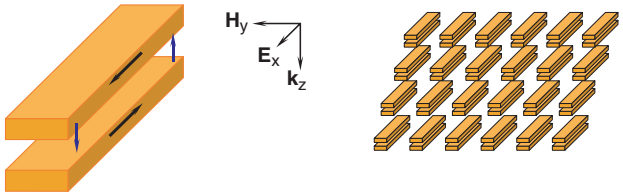

Figure 1 (online color at www.lphys.org) An array of nanorods pairs

in a passive medium. Recently a design of such metamaterials for the microwave spectral range, using metal split ring resonators and thin metal wires, was proposed theoretically [5,6] and realized in microwave experiments [7]. In this letter we demonstrate an *optical* NIM based on coupled metal rods that was previously predicted theoretically [8,9]. The negative refractive index is verified by direct

* Corresponding author: e-mail: shalaev@purdue.edu

phase and amplitude measurements near the communication wavelength of 1.5 μm along with 3D finite difference time domain simulations [10].

Fig. 1 schematically shows the array of closely-spaced pairs of parallel metal nanorods used in our experiments. The two parallel rods form an open current loop, which acts as a transmission line and has a current resonance. Such a loop is "closed" through the displacement current (blue (vertical) arrows in Fig. 1), and it therefore supports the resonant modes of both the electric and magnetic components of light. For normally-incident light with the electric field polarized along the rods and the magnetic field perpendicular to the pair, the electric and magnetic responses both can experience a resonant behavior at certain frequencies that depend on the rod dimensions and their separations. Above the resonance frequency, the circular current in the pair of rods can lead to a magnetic field opposing the external magnetic field of the light, hence enabling a negative magnetic response. In this design, the electric component of the incident wave excites a symmetric current mode in the two metal rods, whereas the magnetic field component excites an anti-symmetric mode (see Fig. 1). The excitation of such plasmon resonances for both the electric and magnetic light components results in the resonant response of the refractive index, which can become negative above the resonance as previously predicted [8,9]. This resonance can be thought of as a resonance in an optical LC-circuit, with the inductance L provided by the metal rods and the dielectric gaps between the rods acting as capacitive elements C. A similar approach to optical NIMs, employing circular currents in two metal plates arranged along the wavevector of incident light, was realized in the near IR range for a system of paired dielectric voids in a metal [11]. We note that this inverted system, i.e. elliptical or rectangular dielectric voids in metal films [12], are physically equivalent to paired metal rods in a dielectric host, in accordance with the Babinet principle.

In parallel with progress for metal-dielectric metamaterials, two experimental demonstrations of negative refraction in the near IR range have been made in photonic crystals (PCs) [13,14]. Light propagation through an interface that mimics negative refraction has been found in two-dimensional PCs [13]. It has been shown that under certain conditions, unique focusing effects in PCs are also possible [14].

2. Fabrication

We study single layer samples fabricated on two different substrates using electron beam lithography (EBL). By varying the substrate material and metal coverage, important quantitative changes in the refractive index, including a change in the index sign are observed.

Experimental results described below were obtained using a 2 mm $\times$ 2 mm array of nanorods. Fig. 2a shows a field-emission scanning electron microscope (FE-SEM) image of a portion of the sample as well as a closer view

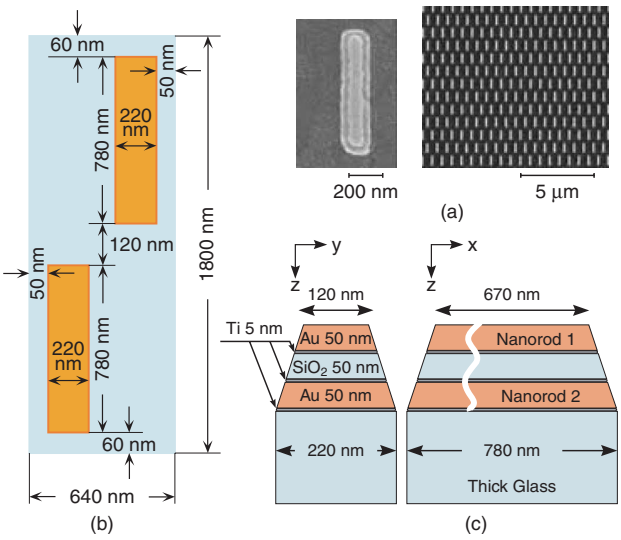

Figure 2 (online color at www.lphys.org) (a) Field-emission SEM images (top view) of a single pair of nanorods (left) and a fragment of 2 mm $\times$ 2 mm array of pairs of nanorods (right). (b) Elementary cell dimensions, and (c) dimensions for a pair of nanorods on glass substrate

of a single pair of rods. A schematic for the whole sample is given in Fig. 2b and Fig. 2c.

The first sample (Sample A) was fabricated on a 180-nm layer of indium tin oxide (ITO) coated onto glass. ITO coating is typically used in EBL to avoid the charging effects of the resist layer under e-beam writing. Before applying the photo-resist for electron beam writing, the ITO-coated glass substrate was cleaned and baked at 160°C for 30 minutes. Next, a double layer of poly(methylmetacrylate) photo-resist was coated onto the ITO-glass substrate. A JEOL JBX-6000FS electron beam writer with optimized dosage was used for writing. After the photo-resist was developed, the desired sandwich structure of metal rods and silicon dioxide (SiO_2) was deposited in an electron beam evaporator at high vacuum. The thickness and sequence of the sandwich structure on the ITO-glass substrate are as follows: 5 nm of titanium (Ti), 50 nm of gold (Au), 5 nm of Ti, 50 nm of SiO_2, 5 nm of Ti and finally 50 nm of Au. A lift-off process was then performed to obtain the array of paired nanorods.

Another sample of the same structure (Sample B) was fabricated on glass without the ITO layer. To prevent the charging effect in this case a thin Cr layer was deposited on top of the resist layer. Then after e-beam writing, the Cr layer was removed with appropriate etching. For both samples, the fabrication resulted in rods that were trapezoidal in shape (with a top-down width difference of 20 nm for each rod). Figs. 2b and 2c show the dimensions of Sample B. Specifically, Fig. 2b shows the sizes (780 nm $\times$ 220 nm) of the bottom rods; the top rods are different in size and they are 670 nm $\times$ 120 nm. This size difference is also clearly seen in Fig. 2a for the single rod pair. The sizes

of the elementary cell for Sample B are slightly less than for Sample A; specifically, they are 1800 nm × 640 nm (Fig. 2b). The metal filling factor for Sample B is 13.5% which exceeds the 8.3% filling factor for Sample A.

3. Experiments and refractive index retrieval

For a transparent optical material of thickness Δ, the phase shift ϕ_t of the transmitted wave is equal to $2\pi n'\Delta/\lambda$ so that $n' < 0$ results in $\phi_t < 0$. In experiments using interferometry, the phase shift in a material can be precisely measured relative to a layer of air (reference) of the same thickness:$\phi_{t,\mathrm{exp}} = \phi_t - \phi_r$, where the phase shift in air is $\phi_r = 2\pi\Delta/\lambda$. Then n' is negative in the material provided that $\phi_{t,\mathrm{exp}} < -\phi_r$. In general, for a metal-dielectric slab with absorption and multiple reflections at the boundary, the relation between ϕ_t and n is more complicated and phase measurements should be accompanied by measurements of the transmittance and reflectance amplitudes. Below we retrieve the refractive index from the exact formula for n; surprisingly, the simple criterion above works rather well for our samples and the refractive index is negative for $\phi_{t,\mathrm{exp}} < -\phi_r$ (this will be discussed in detail elsewhere).

The complex index of refraction (n) of a nanorod layer on a substrate can be found from [17]:

$$\cos nk\Delta = \frac{1 - r^2 + n_s t^2}{(n_s + 1)\, t + rt\,(n_s - 1)}\,, \qquad (1)$$

where n_s is the refractive index of the substrate ($n_s = 1.48$ for our bare glass substrate).

Eq. (1) provides the solution for retrieving the refractive index of a given thin layer of a passive material ($n'' > 0$ and $Z' > 0$, where $Z = Z' + iZ''$ is the impedance) with unknown parameters. Specifically, we obtain the impedance (not shown here) and the refractive index of the equivalent homogeneous layer with the same complex reflectance r and transmittance t as the actual array of nanorods. Such a homogeneous layer with equivalent n and Z gives the same far-field distribution outside the sample as the actual layer of metamaterial. Note that for a thin layer such retrieval can be performed unambiguously.

The amplitudes and phases for transmittance and reflectance needed for retrieval of the refractive index with the use of formula (1) were directly measured in the experiments as described below.

The transmission ($T = |t|^2$) and reflection ($R = |r|^2$) spectra are measured with a Lambda 950 spectrophotometer from Perkin-Elmer using linearly polarized light. The transmission spectra are collected at normal incidence, and the reflection spectra are measured at a small incident angle of 8°. Control measurements of the reflectance performed with a laser source at 0.5° of the incident angle show no significant difference.

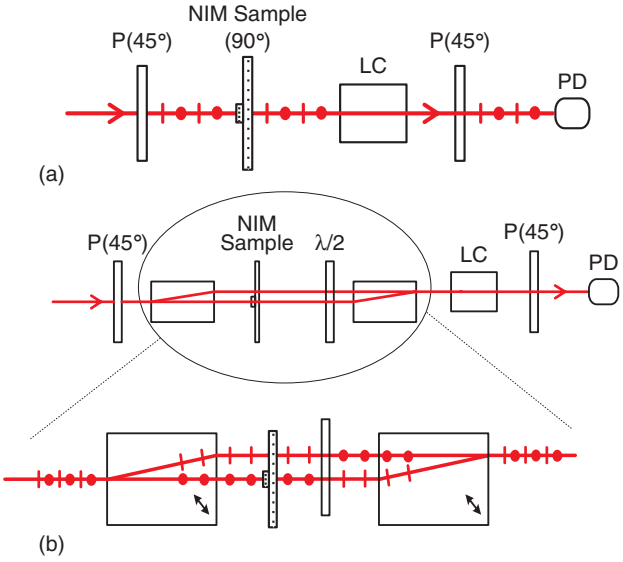

Figure 3 (online color at www.lphys.org) Polarization (a) and walk-off (b) interferometers in transmission mode. P- polarizer, LC- liquid crystal variable phase plate, PD- photodetector, $\lambda/2$-tunable half-wave phase plate. Orthogonal polarizations of light are shown by dots and lines

We performed phase measurements in both transmission and reflectance using polarization and walk-off interferometers and a set of tunable diode lasers. These interferometry methods provide high precision and they are capable of revealing that the phase and group velocities of light are antiparallel in NIMs.

In the polarization interferometer (Fig. 3a), two optical channels have a common geometrical path and differ by the polarization of light. This allows one to measure the phase difference between orthogonally-polarized waves $\Delta\phi = \phi_\parallel - \phi_\perp$ caused by anisotropy of a refractive material. Note that the phase acquired in the substrate does not contribute to the phase difference $\Delta\phi$.

The walk-off interferometer (Fig. 3b) has two optical channels which differ in geometrical paths; it gives a phase shift introduced by a sample (ϕ_s) relative to a reference (ϕ_r):$\delta\phi = \phi_s - \phi_r$. A layer of air with the same thickness as the layer of rods was used as the reference. Both the reference and sample beams go through the substrate so that the phase acquired in the substrate does not contribute to the measured phase shift $\delta\phi$ if the substrate has no variations in optical thickness. The walk-off effect in calcite crystals is employed to separate the two beams and then bring them together to produce interference as is shown at the bottom of Fig. 3b. The phase shifts $\delta\phi_\parallel$ and $\delta\phi_\perp$ are measured for the two light polarizations and their difference is compared with the phase anisotropy $\Delta\phi$ obtained from polarization interferometry (note that $\Delta\phi = \delta\phi_\parallel - \delta\phi_\perp$).

The instrumental error of the phase anisotropy measurement by polarization interferometer is $\pm 1.7°$. We note

that variations in the substrate thickness do not affect the results of our phase anisotropy measurements, which is typical for common path interferometers. In the case of the walk-off interferometer, the thickness variation gives an additional source of error, causing the error for the absolute phase shift measurements to increase up to $\pm 4^\circ$.

We note here two important details of the measurements. First, by varying a lateral position of the sample relative to the optical beam the phase shift is smoothly changed from zero (when the beam is outside of the sample) to the measured value (when the beam is at the sample center). This control eliminates the 2π uncertainty in phase measurements. Secondly, the linear polarization of light is well preserved after propagation through the sample for both light polarizations, parallel and perpendicular to the rods. Specifically, the light ellipticity (the intensity ratio for the two components) changes only from 10^{-3} to 3×10^{-3} after propagation through the sample. Thus we can conclude that the method used provides direct measurements of the magnitude and sign of the phase shift, for the two linearly polarized components of light. This is in contrast to the phase determination without interferometers used in [11], which is indirect and requires *a priori* knowledge of the sample.

4. Simulations

Along with the experimental studies, the optical properties of both samples were simulated using 3D FDTD approach [16]. Our modeling was mainly focused on adequate integration of frequency-dependent permittivity in the general 3D FDTD evolution equation.

To simulate the permittivity, the matching Debye models were obtained from the Drude models for the gold nanorods,

$$\varepsilon_{\mathrm{Au}} = 9.0 - \frac{(1.3673 \times 10^{16})^2}{\omega^2 + i(1.0027 \times 10^{14})\omega}$$

and ITO,

$$\varepsilon_{\mathrm{ITO}} = 3.4626 - \frac{(2.9134 \times 10^{15})^2}{\omega^2 + i(1.5030 \times 10^{14})\omega},$$

where $\omega = 2\pi c/\lambda$. For both materials, these formulas provide excellent agreement with the measured optical constants in the spectral range of interest.

We set the elementary cell with $x \times y \times z = 1900$ nm $\times 700$ nm$\times 4000$ nm for Sample A and $x \times y \times z = 1800$ nm$\times 640$ nm$\times 4000$ nm for Sample B. Both samples were illuminated by a monochromatic plane wave at normal incidence. Since we used a uniform grid with a spatial resolution of 10 nm, the 5-nm Ti layers (Fig. 2c) were not taken into account in those simulations. The thick glass layer was considered infinite in the simulations with the substrate of ITO-coated glass. Two perfectly matching layers [16], which emulate infinite propagation of the scattered field, were arranged in front of and behind the layer of nanorods. Standard periodic boundary conditions were applied to the elementary cell elsewhere to ensure double periodicity of the entire array. The total-scattered field separation technique was used to obtain the scattered fields [16]. The field data for reflection and transmission coefficients were taken at selected evaluation planes in front of

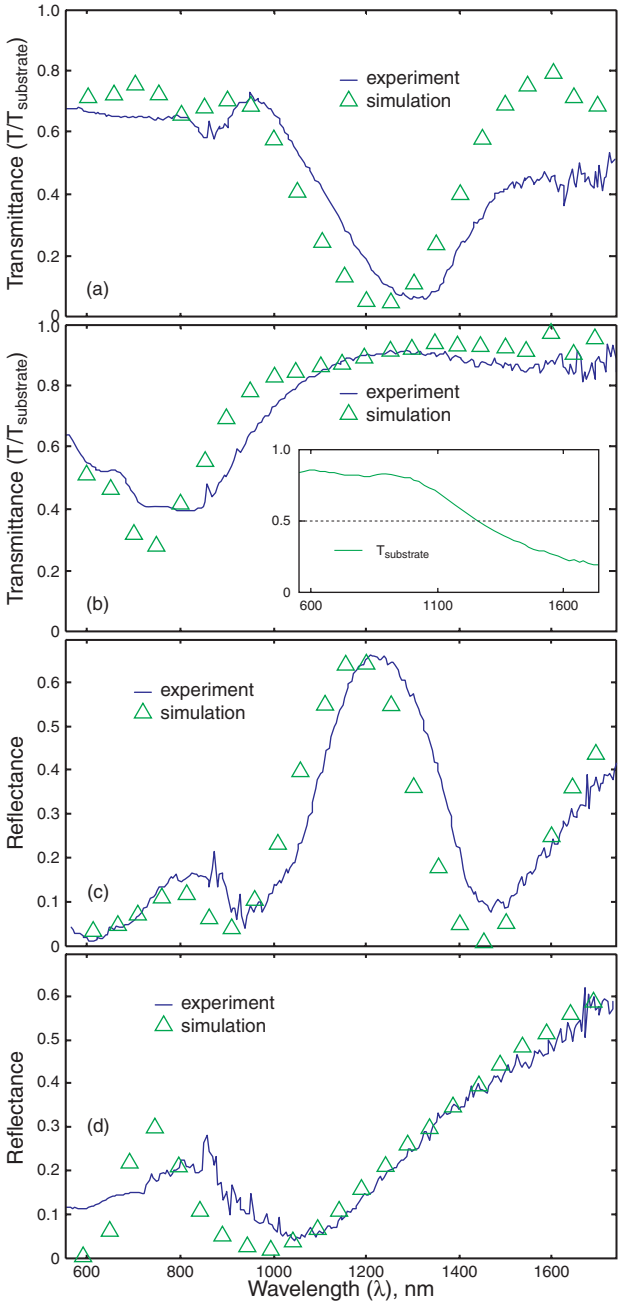

Figure 4 (online color at www.lphys.org) Normalized transmittance $T/T_{substrate}$ ((a) and (b)) and reflectance R ((c) and (d)) of light for Sample A. Two different polarizations are used, one with the electric field along the rods, as in (a) and (c), and one perpendicular to the rods, as in (b) and (d). The transmittance of the substrate (ITO-coated glass) is shown as inset in (b)

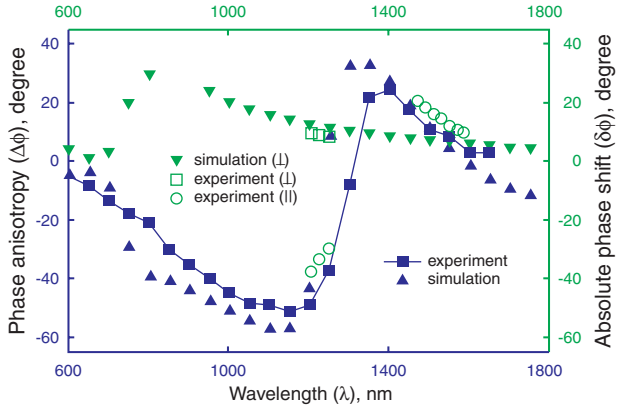

Figure 5 (online color at www.lphys.org) Phase difference in transmission through the layer of pairs of gold rods of Sample A, for light polarized parallel and perpendicular to the rods. The measured (■) and simulated (▲) phase anisotropies $\Delta\phi = \phi_{\parallel} - \phi_{\perp} = \delta\phi_{\parallel} - \delta\phi_{\perp}$ are shown (left ordinate). The absolute phase shifts $\delta\phi_{\parallel}$ and $\delta\phi_{\perp}$ for waves with parallel (◯) and perpendicular (□) polarizations are also depicted (right ordinate). The absolute shifts $\delta\phi_{\perp}$ for the perpendicular polarization are compared to simulation results (▼); $\delta\phi_{\parallel}$ can be found as $\delta\phi_{\parallel} = \Delta\phi + \delta\phi_{\perp}$

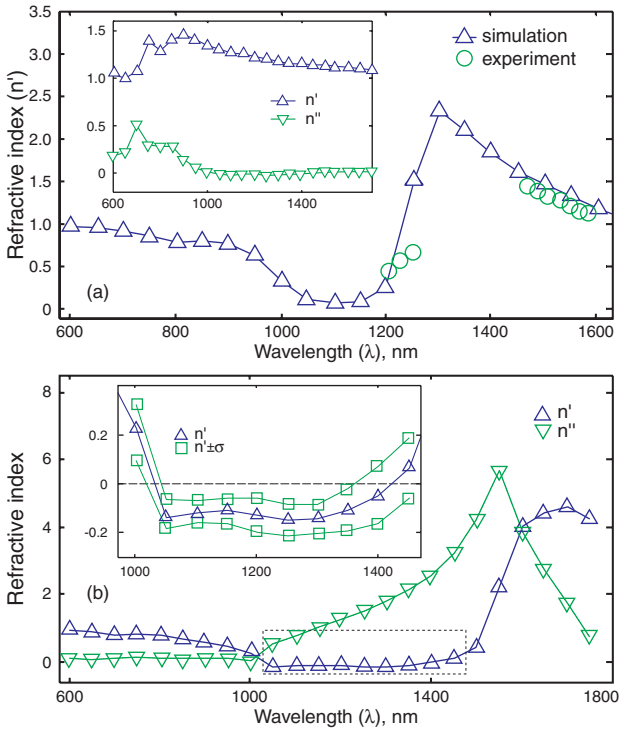

Figure 6 (online color at www.lphys.org) (a) The real part of refractive index for the parallel polarization of incident light restored from measurements and simulations for Sample A. The inset in (a) shows the refractive index calculated for the perpendicular polarization. (b) Refractive index for Sample A simulated without ITO-glass substrate. The inset in (b) shows the zoomed view of Fig. 4b for $n' < 0$, including the upper and lower bounds with a one-sigma deviation

and behind the nanostructure using one-period sampling and additional Fourier filtering with averaging over the evaluation planes.

While the calculations for a given set of wavelengths are only roughly identical in length, for now, the simulations are sped-up by a simple process parallelized approach (different wavelengths are distributed to different CPUs with no special efforts for load balancing). The code is parallelized using the standard Message Passing Interface library.

In our simulations the overall geometry of the nanorods inside the elementary cell followed the trapezoidal shape of the experimental samples. The complex values of the reflected and transmitted electric fields, E_r and E_t, are calculated using 3D FDTD for normally-incident light with electric field E_i. Then, $r = \alpha E_r(-d)/E_i(-d)$ and $t = \alpha E_t(d)/E_i(-d)$ are obtained from the field values, where $\alpha = \exp[ik(\Delta - 2d)]$, k is the wavenumber in air and d is the distance from the center of the layer of the paired nanorods, with the total thickness $\Delta = 160$ nm, to the field evaluation planes in front and behind the sample. The distance d is chosen so that the reflected and transmitted waves (E_r and E_t) are plane waves with no more than 1% deviation in magnitudes in the evaluation planes.

5. Results and discussion

Fig. 4 shows results of our experimental measurements of transmittance (top), and reflectance (bottom) for light propagating through a sample with an ITO layer (results for Sample A are shown, as an example). As seen in Fig. 4, the system of parallel gold nanorods shows a strong plasmonic resonance near 1.3 μm for light with the electric field polarized parallel to the rods. In this case, light excites both electric and magnetic responses. For light with the electrical field polarized perpendicular to the rods, the electric (transverse) plasmon resonance occurs near 800 nm. We note good qualitative agreement between our 3D FDTD simulations and experimental data – both the positions and the widths of the resonances are reproduced well.

Fig. 5 illustrates the results of the phase measurements, which are compared with our simulations. Again, we note good agreement between our FDTD simulations and experimental data; the phase shifts at two different wavelength segments are reproduced very well. As seen in Fig. 5, in the spectral range between 1 and 1.6 μm the absolute phase shift $\delta\phi_{\perp}$ measured with respect to the layer of air is positive and nearly flat (close to $+10°$) in magnitude. In contrast, $\delta\phi_{\parallel}$ shows a strong resonant dependence such that the difference $\delta\phi_{\parallel} - \delta\phi_{\perp}$ agrees very

well with our measurements of $\Delta\phi$ using polarization interferometry. According to Fig. 5, the phase difference $\Delta\phi = \phi_{\parallel} - \phi_{\perp} = \delta\phi_{\parallel} - \delta\phi_{\perp} \approx -50^{\circ}$ and the phase shift $\delta\phi_{\parallel} = \Delta\phi + \delta\phi_{\perp} \approx -40^{\circ}$ at 1.2 μm. The simple qualitative criterion discussed above requires that the experimental phase shift is less than $-\phi_0 = -2\pi\Delta/\lambda = -49^{\circ}$ at 1.2 μm, so the observed $\delta\phi_{\parallel}$ suggests that the refractive index is expected to be close to zero but positive in this case.

To retrieve the exact values of the refractive index we generalized Eq. (1) for a multi-layer system, following the approach of [15], and took into account the ITO layer [17]. Fig. 6a shows the obtained index and demonstrates excellent agreement between measurements and simulations. As expected, the refractive index is close to zero between 1 and 2 μm (the lowest n' is 0.08 at 1.1 μm) but it remains positive. Clearly, the system of parallel gold nanorods shows a strong plasmonic resonance near 1.3 μm for light with the electric field polarized parallel to the rods. In this case, light excites both electric and magnetic responses, resulting in the anomalously low refractive index.

To further quantitatively understand the effect of the substrate, the refractive index was calculated for the same nanorod array but in free space, i.e., *without* the substrate ($n_s = 1$ in Eq. (1)). Our results show a negative n' in this case. The refractive index is negative in the range between 1.1 μm and 1.4 μm, reaching a magnitude of $n' \approx -0.15$ at $\lambda = 1.25$ μm (see Fig. 6b). The imaginary part of the refractive index also shows resonant behavior and it is large near the resonance. Our calculations show that by optimizing the system, the ratio of the real and imaginary parts of the refractive index can be significantly increased. One of ways to decrease losses is to use silver structures (instead of gold) with nanorods of smaller sizes. The transmittance can be also further increased by matching the impedances.

A negative refractive index was obtained for Sample B, containing a similar array of nanorods fabricated directly on glass. As mentioned, the sizes of the lower nanorods in Sample B are slightly larger than in Sample A. The larger rod sizes resulted in a small shift of the resonance toward longer wavelengths, as seen in Fig. 7. In Fig. 7a we show the results of our phase measurements for Sample B. The detected phases are in excellent agreement with simulations. The inset in Fig. 7a depicts the measured transmittance and reflectance magnitudes (for the parallel polarization) verified with the diode laser in the spectral range of interest where n is negative. Fig. 7b exhibits n' obtained with the use of Eq. (1). n'' is similar to that in Fig. 6 and not shown here. Our simulations for both Sample A and B suggest a relatively weak sensitivity of n' to variations in reflectance and transmittance amplitudes and its critical dependence on phases. The excellent agreement between calculated and measured phase shifts resulted in close values for the simulated and experimental values of n'. We note that the obtained absolute phase shift of -61° (not shown) in the light transmittance at $\lambda = 1.5$ μm is well below the critical phase $-\phi_0 = -40^{\circ}$ at 1.5 μm, so the

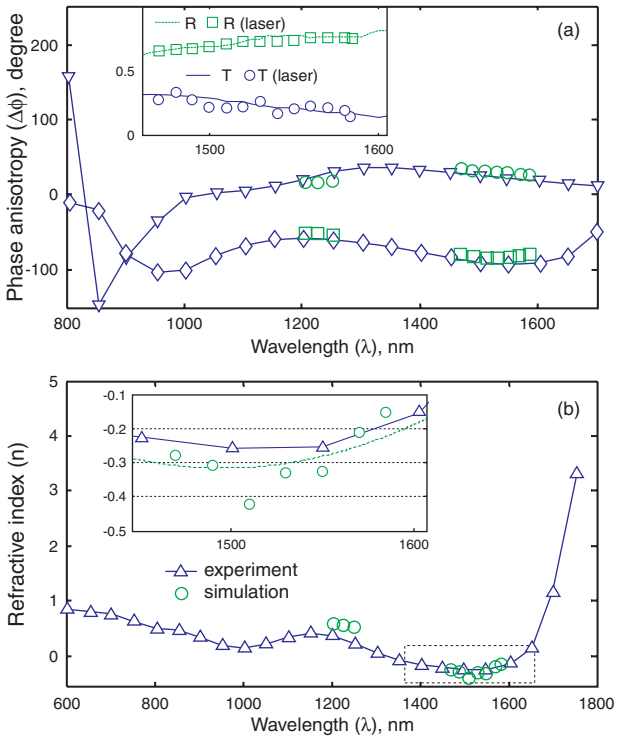

Figure 7 (online color at www.lphys.org) Sample B: (a) Phase anisotropy $\Delta\phi = \phi_{\parallel} - \phi_{\perp}$ for transmitted ($\Diamond$ simulation and $\square$ experiment) and reflected ($\triangledown$ simulation and $\bigcirc$ experiment) light. The inset in (a) shows measured transmittance and reflectance magnitudes for the parallel polarization verified with laser measurements. (b) The real part of the refractive index restored from experimental data and compared to simulations. The inset depicts a zoomed view of the region of negative refraction; the dashed line represents the quadratic least-square fit for experimental data ($\bigcirc$) and the solid line shows the simulated data ($\triangle$)

phase criterion used above also predicts negative refraction in this case. The refractive index is negative between 1.3 μm and 1.6 μm, with $n' = -0.3 \pm 0.1$ at $\lambda = 1.5$ μm. The spectral range of negative n' is shifted with respect to the resonance providing a rather high transmittance of about 20%.

Both examples demonstrate that the array of paired nanorod causes a significant decrease in refractive index for the parallel polarization above the resonance. A different substrate (glass instead of ITO) and a slightly larger metal filling factor resulted in the observed difference in magnitude and sign of the refractive index.

It is interesting to compare the normalized magnetic field distribution for our two samples. Fig. 8 depicts a map of the calculated magnetic field component (H_y), which is collinear with the incident magnetic field. The incident field in both cases has a magnitude of one and has a phase of zero at the center of the pair of rods (shown by the black outline). As predicated by theory, the circular current in the rod pair generates induced magnetic field which

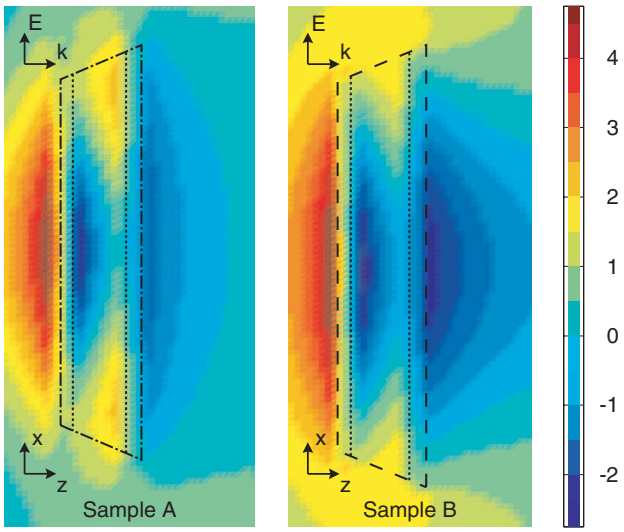

Figure 8 (online color at www.lphys.org) Cross-sectional field map of the magnetic field collinear to the incident magnetic field for Samples A and B. Both diagrams show xz-cross sections through the middle of the nanorod pair

is directed against the incident magnetic field, which is directed against the incident magnetic field. For both samples, the resultant (i.e. the sum of the incident and induced) magnetic field reaches its maximum in the gap between the rod pair and is directed against the incident field. In contrast to Sample A, where the reversed negative field in the middle is almost compensated by the positive field at the edges, in Sample B the negative magnetism is stronger, demonstrating both a wider and deeper area of field reversal.

In conclusion, for an array of pairs of parallel gold rods, we obtained a negative refractive index of $n' \approx -0.3$ at the optical communication wavelength of 1.5 μm. The frequency for negative refraction depends on both the size of the metal rods and their separation and it can span the visible and near-infrared parts of the spectrum through appropriate nanorod array design. Further optimization of the proposed structures would allow NIMs with lower losses and larger magnitudes of negative refraction, resulting in new applications based on this unique phenomenon.

Acknowledgements This work was supported in part by NSF-NIRT award ECS-0210445 and by ARO grant W911NF-04-1-0350. G. Klimeck and the cluster computers (Pentium 4, 3 GHz dual processor machines with 2 GB or RAM) used in this work are supported by the National Science Foundation under Grant No. EEC-0228390, the Indiana 21st Century fund, and the Lilly Foundation.

References

[1] J.B. Pendry, Phys. World **14**, 47 (2001).
[2] J.B. Pendry, Phys. Rev. Lett. **85**, 3966 (2000).
[3] V.G. Veselago, Sov. Phys. Usp. 10, 509 (1968); V.G. Veselago, Usp. Fiz. Nauk **92**, 517 (1964).
[4] R.A. Depine and A. Lakhtakia, Microwave Opt. Tech. Lett. **41**, 315 (2004).
[5] J.B. Pendry, A.J. Holden, W.J. Stewart, and I. Youngs, Phys. Rev. Lett. **76**, 4773 (1996).
[6] J.B. Pendry, A.J. Holden, D.J. Robins, and W.J. Stewart, IEEE Trans. Microwave Theor. Tech. **47**, 2057 (1999).
[7] R.A. Shelby, D.R. Smith, and S. Schultz, Science **292**, 77 (2001).
[8] V.A. Podolskiy, A.K. Sarychev, and V.M. Shalaev, J. Nonlin. Opt. Phys. Mater. **11**, 65 (2002).
[9] V.A. Podolskiy, A.K. Sarychev, and V.M. Shalaev, Opt. Express **11**, 735 (2003).
[10] V.M. Shalaev, W. Cai, U. Chettiar, et al., http://arxiv.org/ftp/physics/papers/0504/0504091.pdf (2005).
[11] S. Zhang, W. Fan, N.C. Panoiu, et al., http://arxiv.org/ftp/physics/papers/0504/0504208.pdf (2005).
[12] S. Zhang, W. Fan, K.J. Malloy, et al., Opt. Express **13**, 4922 (2005).
[13] A. Berrier, M. Mulot, M. Swillo, et al., Phys. Rev. Lett. **93**, 73902 (2004).
[14] E. Schonbrun, M. Tinker, W. Park, and J.-B. Lee, IEEE Photon. Tech. Lett. **17**, 1196 (2005).
[15] D.R. Smith, S. Schultz, P. Markos, and C.M. Soukoulis, Phys. Rev. B **65**, 195104 (2002).
[16] A. Taflove and S. Hagness, Computational Electrodynamics: The Finite-Difference Time-Domain Method (Artech, Boston, MA, 2000).
[17] A.V. Kildishev, W. Cai, U.K. Chettiar, et al., J. Opt. Soc. Am. B, to be published; A.V. Kildishev, W. Cai, U.K. Chettiar, et al., http://arxiv.org/ftp/physics/papers/0510/0510001.pdf (2005).